Int J Thermophys (2016) 37:68
DOI 10.1007/s10765-016-2073-x

ICPPP 18

Laser-Generated Lamb Waves Propagation in Multilayered Plates Composed of Viscoelastic Fiber-reinforced Composite Materials

Hong-xiang Sun[1,2,3] · Shu-yi Zhang[1] · Shou-qi Yuan[2] · Yi-jun Guan[2] · Yong Ge[2]

Received: 29 October 2015 / Accepted: 28 April 2016 / Published online: 14 May 2016

Abstract The propagation characteristics of laser-generated Lamb waves in multilayered fiber-reinforced composite plates with different fiber orientations and number of layers have been investigated quantitatively. Considering the viscoelasticity of the composite materials, we have set up finite element models for simulating the laser-generated Lamb waves in two types of the multilayered composite plates. In the first type, different fiber orientations are adopted. In the second one, different number of layers are considered. The results illustrate the occurrence of attenuation and dispersion, which is induced by the viscoelasticity and multilayer structure, respectively.

Keywords Composite materials · Finite element simulation · Lamb waves · Laser ultrasound · Multilayered plate · Viscoelasticity

1 Introduction

Laser ultrasound (LU) has been widely studied and applied to nondestructive evaluation of materials and devices [1–6]. In the study of LU in the fiber-reinforced composite

This article is part of the selected papers presented at the 18th International Conference on Photoacoustic and Photothermal Phenomena.

✉ Hong-xiang Sun
jsdxshx@ujs.edu.cn

1 Lab of Modern Acoustics, Institute of Acoustics, Collaborative Innovation Center of Advanced Microstructures, Nanjing University, Nanjing 210093, China

2 Faculty of Science, Jiangsu University, Zhenjiang 212013, China

3 State Key Laboratory of Acoustics, Institute of Acoustics, Chinese Academy of Sciences, Beijing 100190, China

materials, the anisotropic and viscoelastic properties of the materials are strongly affecting the propagation characteristics of ultrasonic waves [7–10]. Recently, laser-generated Lamb waves in thin plates have been investigated numerically by introducing complex-valued elastic moduli in order to incorporate viscoelasticity [11,12]. In addition, by considering both anisotropic and viscoelastic properties of the fiber-reinforced composites, laser-generated ultrasonic waves in the single layer plates [7–9] and coating/substrate systems [10] have been studied, but in which the fiber orientations are parallel in these structures. Practically, in order to enhance the mechanical properties, some composites are made of multilayered fiber plates, in which the fiber orientations of various layers are different from one another. Therefore, it is important to study the laser-generated ultrasonic waves in the multilayered composite plates with different fiber orientations.

In this paper, based on the plane strain theory, finite element (FE) models for simulating the laser-generated Lamb waves in two types of multilayered composite plates with viscoelasticity are developed, in which different fiber orientations are adopted in the first type and different layer numbers are applied in the second type. The effects of the fiber orientations and layer number on the propagation characteristics of the laser-generated Lamb waves are investigated in detail.

2 Plane Strain Theory

We consider a multilayered composite plate made of the carbon fiber-reinforced epoxy matrix (Ca-Ep) composite with two types of fiber orientations 0° and 90° which are corresponding to the fiber directions being parallel and perpendicular to the x direction, respectively. The focused pulsed laser line source is assumed to be oriented along the z direction, producing non-zero displacements in both x and y directions. Therefore, the structure can be simplified as the two-dimensional (2D) model as shown in Fig. 1a, where the symmetrical left half is omitted. The thickness of each layer is the same as the diameter (d) of the carbon fiber. If the fibers are normal to x direction (fiber orientation 90°), the governing motion equations in the fiber layer are expressed in the frequency domain as follows [13]

$$\begin{cases} C_{11}^{*}\frac{\partial^2\tilde{u}}{\partial x^2} + C_{66}^{*}\frac{\partial^2\tilde{u}}{\partial y^2} + (C_{12}^{*} + C_{66}^{*})\frac{\partial^2\tilde{v}}{\partial x\partial y} + \rho\omega^2\tilde{u} = 0 \\ C_{22}^{*}\frac{\partial^2\tilde{v}}{\partial y^2} + C_{66}^{*}\frac{\partial^2\tilde{v}}{\partial x^2} + (C_{12}^{*} + C_{66}^{*})\frac{\partial^2\tilde{u}}{\partial x\partial y} + \rho\omega^2\tilde{v} = 0 \end{cases}, \tag{1}$$

where $\tilde{u}$ and $\tilde{v}$ are the Fourier transforms of the displacements in the x and y directions, respectively, ρ is the density, ω is the angular frequency, and $C_{ij}^{*} = C_{ij}' + \mathrm{i}C_{ij}''(i, j = 1, 2, \ldots, 6)$ are defined as the complex moduli, in which C_{ij}' and C_{ij}'' represent the elastic and viscous moduli, respectively.

In addition, if the fibers are along x direction (fiber orientation 0°), the moduli C_{ij}^{*} in Eq. 1 are replaced as follows C_{11}^{*} by C_{33}^{*}, C_{66}^{*} by C_{55}^{*}, and C_{12}^{*} by C_{13}^{*} [9], and the other parameters are the same as those in the fiber layer with the orientation 90°.

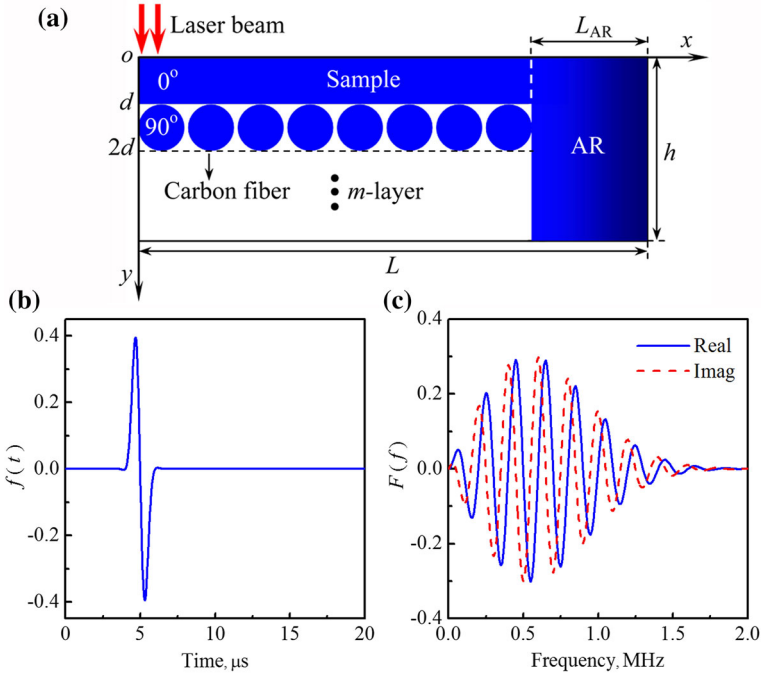

Fig. 1 (a) Geometry diagram of numerical model, and (b) exciting source and (c) its frequency spectrum

3 FE Model and Parameters

Based on the aforementioned equations, we have established the FE model to numerically simulate the laser-generated Lamb waves in the multilayered composite plates by COMSOL Multiphysics software, and Eq. 1 is written in FE-code form as following [14]

$$\nabla \cdot (c\nabla \tilde{U}) - a\tilde{U} = 0, \tag{2}$$

where $\nabla = (\frac{\partial}{\partial x}, \frac{\partial}{\partial y})$, $\tilde{U} = (\tilde{u}, \tilde{v})$, c is a 2×2 matrix composed of four sub-matrices expressed as

$$\begin{aligned} c_{11} &= \begin{pmatrix} C_{11}^* & 0 \\ 0 & C_{66}^* \end{pmatrix} \quad c_{12} = \begin{pmatrix} 0 & C_{12}^* \\ C_{66}^* & 0 \end{pmatrix} \\ c_{21} &= \begin{pmatrix} 0 & C_{66}^* \\ C_{12}^* & 0 \end{pmatrix} \quad c_{22} = \begin{pmatrix} C_{66}^* & 0 \\ 0 & C_{22}^* \end{pmatrix} \end{aligned}, \tag{3}$$

and a is a 2×2 matrix given by

$$a = \begin{pmatrix} -\rho\omega^2 & 0 \\ 0 & -\rho\omega^2 \end{pmatrix}. \tag{4}$$

The stress and displacements are continuous at each interface, and stress-free boundary conditions are adopted at top and bottom surfaces of the multilayered composite plate. Moreover, to avoid undesired reflections from the right side of the 2D model, fictitious viscoelastic properties are introduced to realize the absorbing region (AR) [11,12] so that the model represents the behavior of a semi-infinite structure. Moreover, the initial displacement, velocity, and acceleration equal zero.

The geometrical parameters shown in Fig. 1a are listed as follows: $d = 0.1$ mm, $L = 40$ mm, and $L_{\mathrm{AR}} = 10$ mm. The material parameters of the Ca-Ep are listed as follows: $\rho = 1820\,\mathrm{kg/m^3}$, $C_{11}^* = 12 + \mathrm{i} * 0.8$ GPa, $C_{22}^* = 12 + \mathrm{i} * 0.8$ GPa, $C_{33}^* = 140 + \mathrm{i} * 10$ GPa, $C_{12}^* = 5.4 + \mathrm{i} * 0.4$ GPa, $C_{13}^* = 6.0 + \mathrm{i} * 0.9$ GPa, $C_{55}^* = 6.2 + \mathrm{i} * 0.4$ GPa, and $C_{66}^* = 3.3 + \mathrm{i} * 0.2$ GPa [13].

In the model, we have neglected the thermoelastic effect of the pulsed laser source, and adopted the equivalent stress of the pulsed laser as an exciting source, which is described as [15–18]

$$f(t) = \frac{2}{\alpha\sqrt{2\pi}} \exp\left[-\frac{(t-t_0)^2}{2\alpha^2}\omega_c^2\right] \sin(\omega_c t), \tag{5}$$

where α is a dimensionless parameter controlling the pulse width, t_0 determines the pulse delay time, and $\omega_c = 2\pi f_c$ is the center angular frequency of the pulse. Here, we choose $\alpha = 1.2$, $t_0 = 5\,\mu$s, and $f_c = 0.5$ MHz. The equivalent stress is located at $x = 0$ on the top surface, and its width is 0.1 mm. Figure 1b, c show the time history of the exciting source and its frequency spectrum, $f\ (t)$ and $F(f)$, respectively.

Meanwhile, the element size L_e is very important for the stability and accuracy of the solutions. The element size satisfies the criterion given by [19]

$$L_e \leq \lambda_{\min}/10, \tag{6}$$

where $\lambda_{\min}$ presents the smallest wavelength in the ultrasonic fields. In the FE model, the maximum element sizes are generally arranged to be 20 μm, whereas the element size is 5 μm near the exciting zone, which is much finer for obtaining the transient displacement field accurately.

The spectrum $F(f)$ is used as the exciting source of the FE model in the frequency domain, and the range of $F(f)$ is confined to $0 \leq f \leq 2.0$ MHz as shown in Fig. 1c. The frequency step is arranged to be 0.01 MHz, so the frequency range of $F(f)$ is divided into 200 frequency units. Then the waveforms can be obtained by applying an inverse fast Fourier transform for the displacement spectra predicted from the 200 frequency units.

4 Numerical Results and Discussions

4.1 Four-Layer Composite Plates with Different Fiber Orientations

As the first example, we have simulated the laser-generated Lamb waves in the four-layer composite plates with different fiber orientations, in which the source–receiver

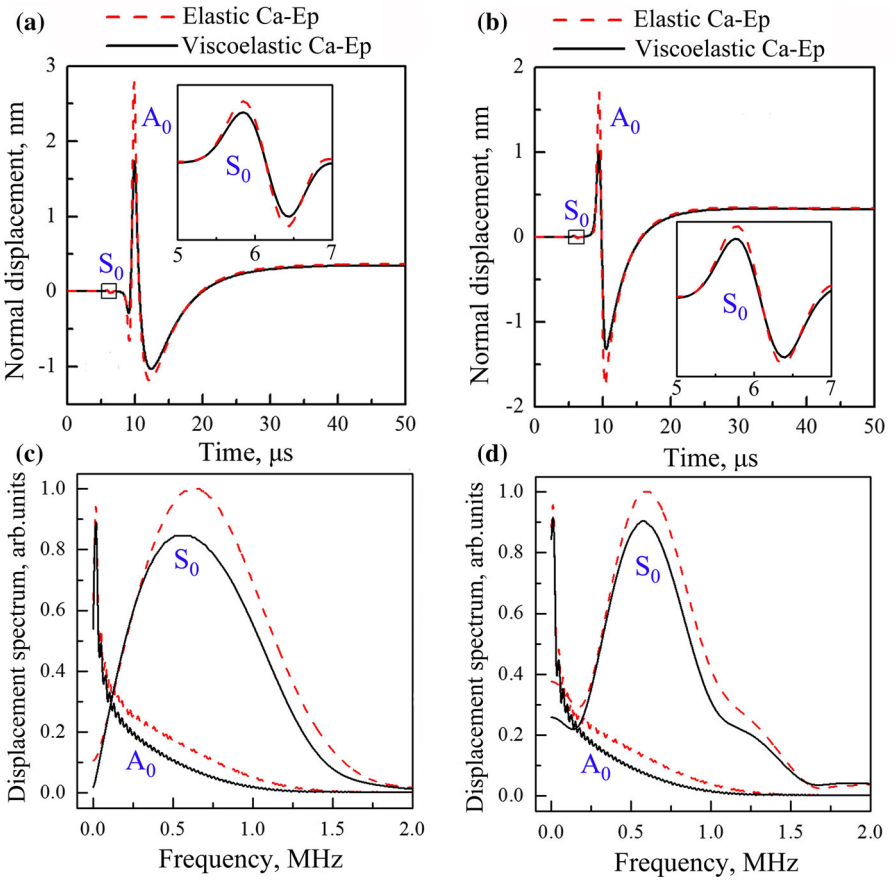

Fig. 2 Normal surface displacements in multilayered composite plates: (a) 90°/0°/0°/0° and (b) 0°/90°/0°/0°, and frequency spectra of S_0 and A_0 modes: (c) 90°/0°/0°/0° and (d) 0°/90°/0°/0°

distance is taken as 10 mm, and the solid and dashed lines represent the displacements with and without the viscoelasticity of the Ca-Ep, respectively.

First, we have considered two kinds of four-layer composite plates, in which the fiber orientations are arranged as one layer 90° and the other three layers 0°. Figure 2a, b show the normal surface displacements in 90°/0°/0°/0° and 0°/90°/0°/0° plates, respectively. The lower frequency components of the Lamb waves, such as the symmetric (S_0) and asymmetric (A_0) modes, are dominant in both plates, and that the amplitudes of the displacements decrease greatly with the viscoelasticity of the Ca-Ep, (solid lines). Comparing the results in Figs. 2a, b, the dispersive characteristic of the A_0 mode in 90°/0°/0°/0° plate is more pronounced than that in 0°/90°/0°/0° plate. Figures 2c, d show the frequency spectra of the S_0 and A_0 modes in above both plates, in which the frequency bandwidth of the S_0 mode in the 90°/0°/0°/0° plate is larger than that in the 0°/90°/0°/0° plate. These results indicate that the position

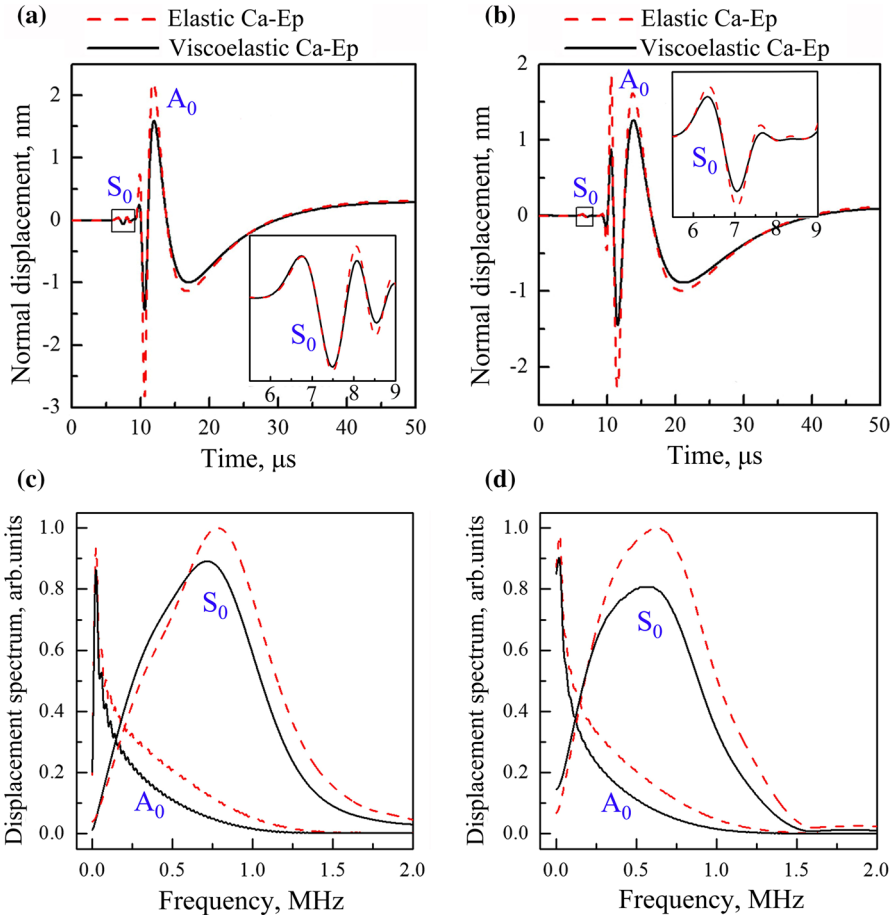

Fig. 3 Normal surface displacement in multilayered composite plates: (a) 0°/90°/90°/90° and (b) 90°/0°/90°/90°, and frequency spectra of S_0 and A_0 modes: (c) 0°/90°/90°/90° and (d) 90°/0°/90°/90°

of the fiber orientation 90° in the composite plate affects the characteristics of the laser-generated Lamb waves.

We have also studied two other kinds of four-layer composite plates composed of one layer 0° and the other three layers 90°, i.e., 0°/90°/90°/90° and 90°/0°/90°/90° plates, and the normal surface displacements are shown in Fig. 3a, b, respectively. Compared with Fig. 2a, b, the dispersive characteristics of the S_0 and A_0 modes become more apparent in Fig. 3a, b. Also, the dispersive characteristic of the S_0 mode in the 0°/90°/90°/90° plate is more obvious than that in the 90°/0°/90°/90° plate, while the dispersive characteristic of the A_0 mode shows inverse situation. Moreover, compared with the results in Fig. 3a, the frequency of the S_0 mode is lower and the attenuation is stronger in Fig. 3b. These characteristics of the S_0 and A_0 modes in both

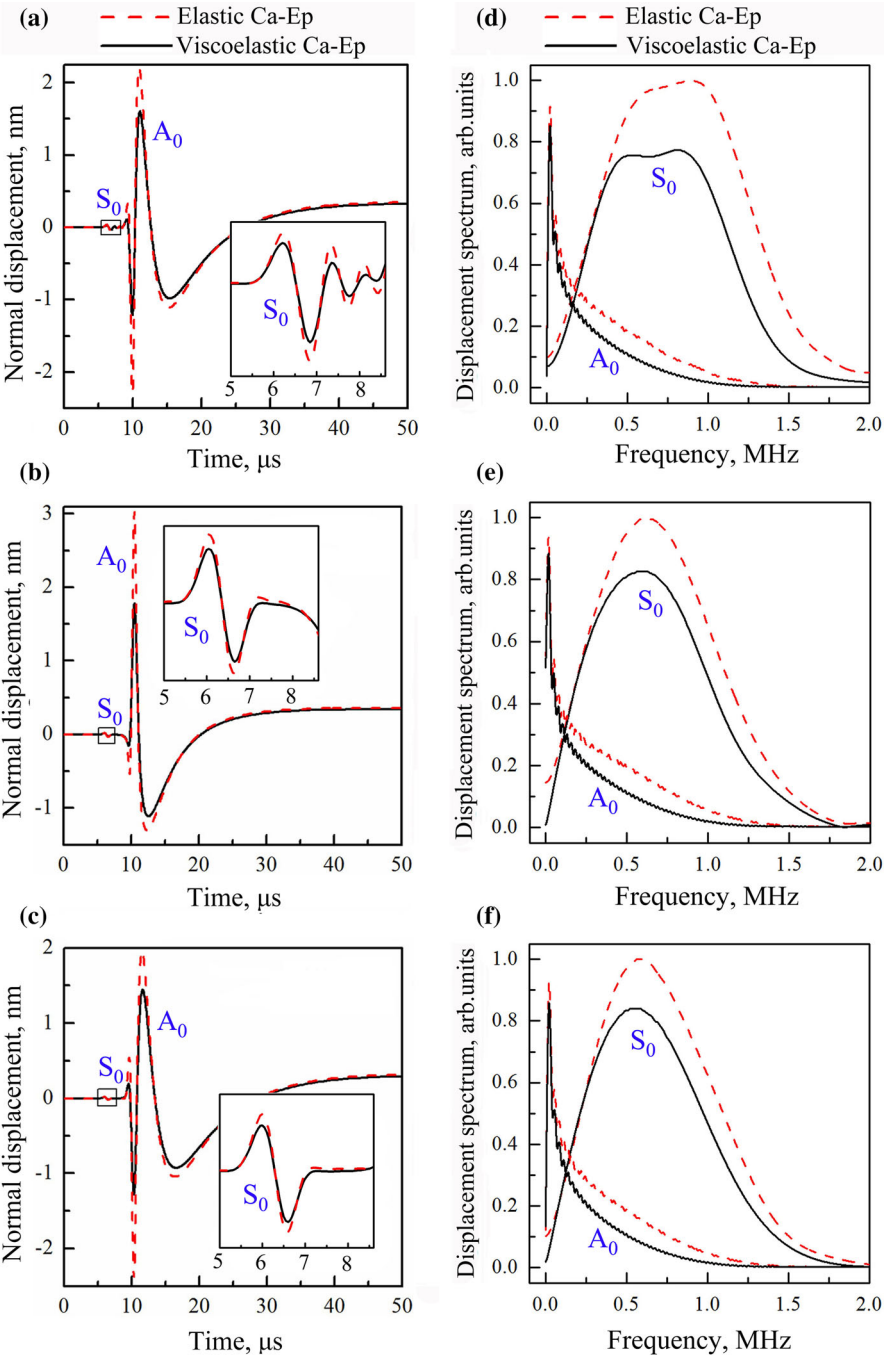

Fig. 4 Normal surface displacements in multilayered composite plates: (a) 90°/90°/0°/0°, (b) 90°/0°/90°/0°, and (c) 90°/0°/0°/90°, and frequency spectra of S_0 and A_0 modes: (d) 90°/90°/0°/0°, (e) 90°/0°/90°/0°, and (f) 90°/0°/0°/90°

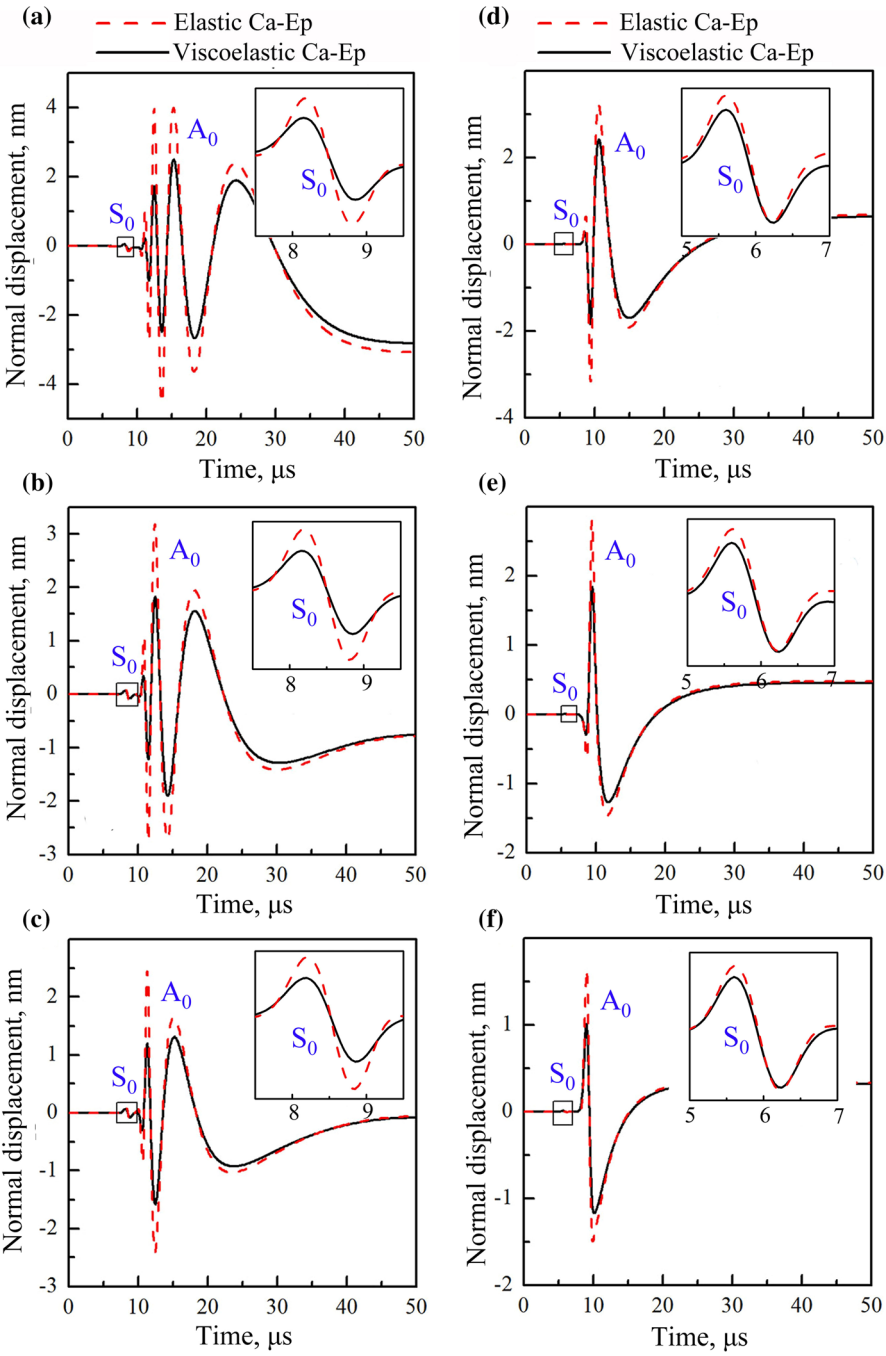

Fig. 5 Normal surface displacements in multilayered composite plates: (a) 90°/90°, (b) 90°/90°/90°, (c) 90°/90°/90°/90°, (d) 0°/0°, (e) 0°/0°/0°, and (f) 0°/0°/0°/0°

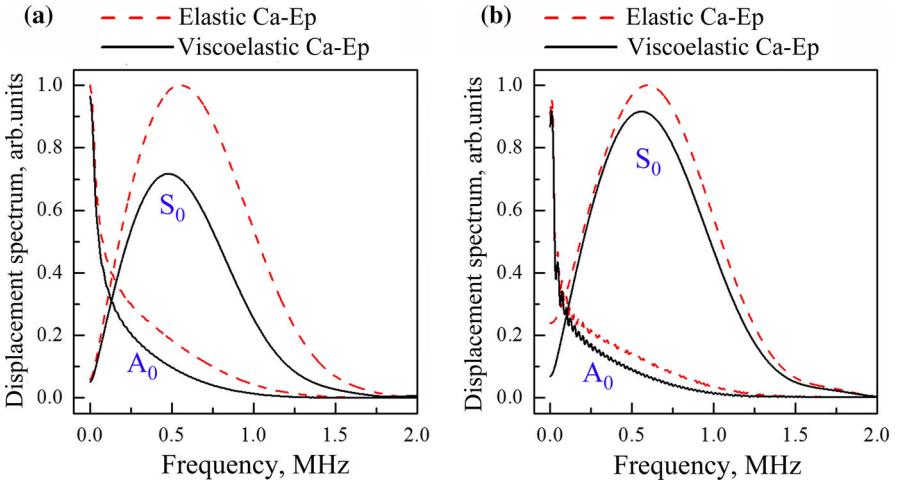

Fig. 6 Frequency spectra of S_0 and A_0 modes: (a) 90°/90°/90°/90° and (b) 0°/0°/0°/0°

types of plates are also presented in the corresponding frequency spectra as shown in Fig. 3c, d.

We have also investigated the four-layer plates with two layers 0° and the others 90°, and the normal surface displacements in three types of plates, such as 90°/90°/0°/0°, 90°/0°/90°/0°, and 90°/0°/0°/90°, are shown in Fig. 4a, c, respectively. Compared with Fig. 4b, c, the dispersive characteristic of the S_0 mode is more pronounced in Fig. 4a. The frequency spectra of the S_0 and A_0 modes corresponding to Fig. 4a–c are depicted in Fig. 4d–f, respectively. The frequency band of the S_0 mode in Fig. 4d is wider than that in Fig. 4e, f, but the characteristics of the A_0 mode are almost the same in the three cases.

In summary, the fiber orientations of the sublayer in the multilayered composite plates turn out to strongly influence the characteristics of the laser-generated Lamb waves.

4.2 Multilayered Composite Plates with Different Number of Fiber Layers

We have also studied the laser-generated Lamb waves in the multilayered composite plates with different number of fiber layers, and the source–receiver distance is also 10 mm. Figure 5a–c present the normal surface displacements in 90°/90°, 90°/90°/90°, and 90°/90°/90°/90° plates, respectively. The degree of dispersive characteristics of the A_0 mode becomes weaker with the increasing number of layers, but the S_0 modes are almost unchanged. Moreover, the results in 0°/0°, 0°/0°/0°, and 0°/0°/0°/0° plates are shown in Fig. 5d–f, and the variation tendency of the A_0 mode is very similar to that in Fig. 5a–c. Compared with Fig. 5d–f, the dispersive characteristics of the A_0 mode are stronger, and the attenuation of the S_0 and A_0 modes is stronger in Fig. 5a–c. In order to clearly show these characteristics, we also calculate the spectra of the S_0 and A_0 modes as shown in Fig. 6a, b, which is corresponding to Fig. 5c, f,

respectively. The attenuation of the S_0 and A_0 modes in Fig. 6b is much smaller than those in Fig. 6a, which agrees well with the results in Fig. 5c, f.

In summary, the results show that the number of layers (≤ 4) in multilayer composite plates mainly affects the dispersion of the A_0 mode.

5 Conclusions

The propagation characteristics of the laser-generated Lamb waves in the multilayered composite plates for different scenarios of the fiber orientations and number of layers have been investigated quantitatively. The results show that the fiber orientations and layer number in the multilayered composite plates have a strong influence on the velocity dispersion and on the attenuation of the laser-generated Lamb waves.

Acknowledgments This work was supported by the National Basic Research Program of China (Grant No. 2012CB921504), Major Program of the National Natural Science Foundation of China (Grant No. 51239005), National Natural Science Foundation of China (Grant No. 11404147), Natural Science Foundation of Jiangsu Province of China (Grant No. BK20140519), China Postdoctoral Science Foundation (Grant No. 2015M571672), Research Fund for Advanced Talents of Jiangsu University (Grant No. 13JDG106), Training Project of Young Backbone Teachers of Jiangsu University, and Special Fund for Public Interest of China (Grant No. 201510068).

References

1. X. Jian, Y. Fan, R.S. Edwards, S. Dixon, J. Appl. Phys. **100**, 064907 (2006)
2. X.D. Xu, J. Goossens, G. Shkerdin, C. Glorieux, I.E.E.E. Trans, I.E.E.E Trans. Ultrason. Ferroelectr. Freq. Control **55**, 675 (2008)
3. C. Grunsteidl, I.A. Veres, J. Roither, P. Burgholzer, T.W. Murray, T. Berer, Appl. Phys. Lett. **102**, 011103 (2013)
4. P. Hess, A.M. Lomonosov, A.P. Mayer, Ultrasonics **54**, 39 (2014)
5. C. Ni, N. Chigarev, V. Tournat, N. Delorme, N. Chigarev, Z. Shen, V.E. Gusev, J. Appl. Phys. **113**, 014906 (2013)
6. J. Jia, Z.H. Shen, K.H. Sun, Appl. Opt. **54**, 7406 (2015)
7. J.J. Wang, B.Q. Xu, Z.H. Shen, X.W. Ni, J. Lu, Jpn. J. Appl. Phys. **47**, 956 (2008)
8. B.Q. Xu, J. Feng, G.D. Xu, J.J. Wang, H.X. Sun, G.R. Cao, Appl. Phys. A **91**, 173 (2008)
9. H.X. Sun, B.Q. Xu, G.D. Xu, C.G. Xu, Chin. Opt. Lett. **8**, 776 (2010)
10. H.X. Sun, S.Y. Zhang, J.P. Xia, Int. J. Thermophys. **36**, 1156 (2015)
11. H.X. Sun, S.Y. Zhang, J. Appl. Phys. **108**, 123101 (2010)
12. H.X. Sun, S.Y. Zhang, Int. J. Thermophys. **34**, 1769 (2013)
13. B. Hosten, M. Castaings, NDT&E Int. **39**, 195 (2006)
14. COMSOL Multiphysics User's Guide, Version 4.3 http://www.comsol.com/
15. O.M. Mukdadi, S.K. Datta, Rev. Prog. Quant. Nondestruct. Eval. **23**, 238 (2004)
16. H.X. Sun, B.Q. Xu, R.Z. Qian, J. Appl. Phys. **106**, 073108 (2009)
17. H.X. Sun, S.Y. Zhang, J. Appl. Phys. **109**, 073107 (2011)
18. H.X. Sun, S.Y. Zhang, Int. J. Thermophys. **36**, 1244 (2015)
19. F. Schubert, B. Koehler, A. Peiffer, J. Comput. Acoust. **9**, 1127 (2001)